TiEMPO: open-source time-dependent end-to-end model for simulating ground-based submillimeter astronomical observations

Esmee Huijten,[a,b,c] **Yannick Roelvink**,[a,b] **Stefanie A. Brackenhoff**,[a,d] **Akio Taniguchi**,[e] **Tom J. L. C. Bakx**,[e] **Kaushal B. Marthi**,[d] **Stan Zaalberg**,[a,b] **Anne-Kee Doing**,[a,b] **Jochem J. A. Baselmans**,[a,f] **Kah Wuy Chin**,[g,h] **Robert Huiting**,[f] **Kenichi Karatsu**,[a,f] **Alejandro Pascual Laguna**,[a,f] **Yoichi Tamura**,[e] **Tatsuya Takekoshi**,[i] **Stephen J. C. Yates**,[j] **Maarten van Hoven**,[a] **and Akira Endo**[a,*]

[a]Delft University of Technology, Faculty of Electrical Engineering, Mathematics and Computer Science, Delft, The Netherlands
[b]Delft University of Technology, Faculty of Applied Sciences, Delft, The Netherlands
[c]Swiss Federal Institute of Technology, Department of Physics, Zurich, Switzerland
[d]University of Groningen, Kapteyn Astronomical Institute, Groningen, The Netherlands
[e]Nagoya University, Graduate School of Science, Division of Particle and Astrophysical Science, Aichi, Japan
[f]SRON—Netherlands Institute for Space Research, Leiden, The Netherlands
[g]National Astronomical Observatory of Japan, Tokyo, Japan
[h]University of Tokyo, School of Science, Department of Astronomy, Tokyo, Japan
[i]Kitami Institute of Technology, Kitami, Hokkaido, Japan
[j]SRON—Netherlands Institute for Space Research, Groningen, The Netherlands

Abstract The next technological breakthrough in millimeter–submillimeter astronomy is three-dimensional imaging spectrometry with wide instantaneous spectral bandwidths and wide fields of view. The total optimization of the focal-plane instrument, the telescope, the observing strategy, and the signal-processing software must enable efficient removal of foreground emission from the Earth's atmosphere, which is time-dependent and highly nonlinear in frequency. Here, we present Time-dependent End-to-end Model for Post-process Optimization (TiEMPO) of the DEep Spectroscopic HIgh-redshift MApper (DESHIMA) spectrometer. TiEMPO utilizes a dynamical model of the atmosphere and parameterized models of the astronomical source, the telescope, the instrument, and the detector. The output of TiEMPO is a time stream of sky brightness temperature and detected power, which can be analyzed by standard signal-processing software. We first compare TiEMPO simulations with an on-sky measurement by the wideband DESHIMA spectrometer, and find good agreement in the noise and sensitivity. We then use TiEMPO to simulate the detection of the line emission spectrum of a high-redshift galaxy using the DESHIMA 2.0 spectrometer in development. The TiEMPO model is open source. Its modular and parametrized design enables users to adapt it to optimize the end-to-end performance of spectroscopic and photometric instruments on existing and future telescopes. [DOI: 10.1117/1.JATIS.8.2.028005]

Keywords: millimeter-wave; astronomy; simulations; submillimeter-wave; kinetic inductance detectors; on-chip spectrometers; atmosphere.

Paper 21134G received Oct. 23, 2021; accepted for publication May 13, 2022; published online Jun. 3, 2022.

*Address all correspondence to Akira Endo, a.endo@tudelft.nl

1 Introduction

The rapidly growing instantaneous bandwidth[1–5] and field-of-view[6–8] of millimeter–submillimeter (mm–submm) astronomical instruments and telescopes are advantageous not only for collecting more astronomical signal but also for characterizing and removing the foreground emission of the Earth's atmosphere.[9] Even at the best sites for submm astronomy on the ground, the brightness temperature of the Earth's atmosphere in the submm range is $\geq$20 K, which can be $\sim 10^3$ to 10^5 times stronger than the astronomical signal (see Fig. 1). Conventional heterodyne instruments on single-dish telescopes have a typical instantaneous bandwidth of several GHz, which is small compared with the atmospheric "windows" (the frequency bands over which the atmosphere is relatively transparent). In this narrow-band case, the effect of the atmosphere can often be approximated with a baseline that is linear in frequency. However, the (ultra-)wideband spectrometers in development, such as the DEep Spectroscopic HIgh-redshift MApper (DESHIMA),[1,2,10] are influenced by the nonlinear frequency dependence of the atmosphere because they measure across one or even multiple atmospheric windows with strong absorption bands in between. On the one hand, this poses new challenges on the observation and signal-processing techniques to remove the nonlinear atmospheric emission.[9] On the other hand, the wideband spectral information of the atmosphere could enable the development and use of advanced signal processing methods for characterizing and ultimately removing the atmospheric component to extract the astronomical signal in a better way.[11,12] The requirements for applying such techniques are expected to drive the design of future telescopes and focal-plane instrument systems.[6–8]

Here, we present the Time-dependent End-to-end Model for Post-process Optimization (TiEMPO) of the DESHIMA spectrometer. TiEMPO is a numerical model for simulating

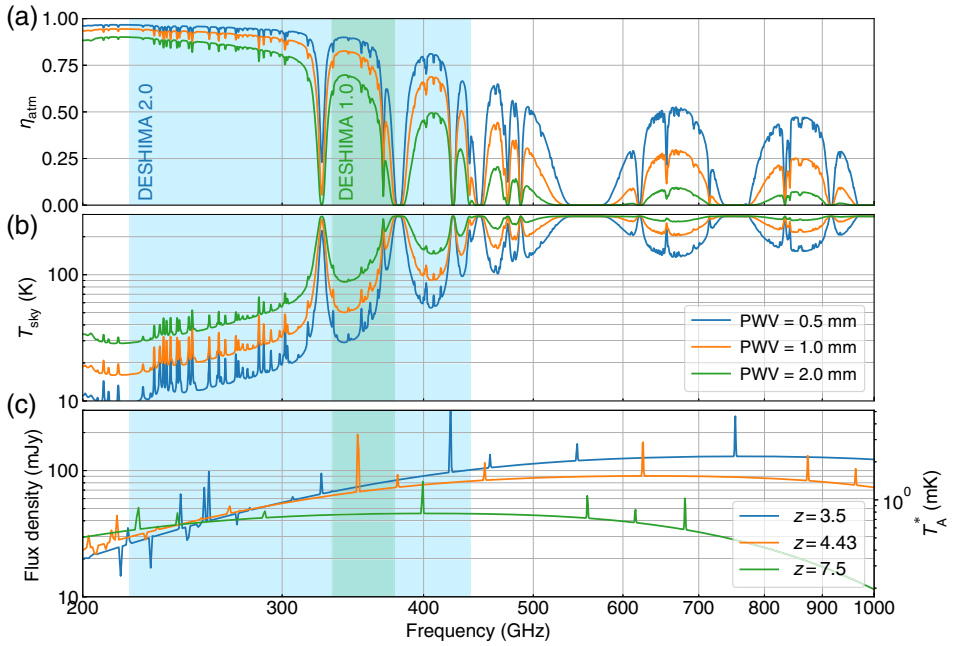

Fig. 1 Atmospheric transmittance η_{atm} (a) and sky brightness temperature T_{sky} (b) at zenith ($\theta = 90$ deg) as functions of frequency, for three values of precipitable water vapor (PWV). The instantaneous frequency coverage of DESHIMA 1.0[1] and the future DESHIMA 2.0 (see Sec. 4) are indicated by the green and blue shades, respectively. The range of DESHIMA 1.0 is an example of one atmospheric "window." DESHIMA 2.0 spans multiple atmospheric windows with absorption-bands in between. (c) GalSpec-simulated spectrum of a galaxy with a far-infrared luminosity of $L_{FIR} = 10^{13.7} L_\odot$, placed at three different redshifts. The spectrum for $z = 4.43$ is given as input to TiEMPO in Sec. 4. The right vertical axis is a rough indication of the corresponding atmosphere-corrected antenna temperature T_A^*, assuming a ∅10 m telescope with an aperture efficiency of 0.6.

wideband submm astronomical observations through the Earth's atmosphere; it produces timestream data that can be fed to data-analysis software[11–13] as if they were taken with a real instrument operated on a telescope. To account for the nonlinear, dynamic, and inhomogeneous transmittance of the atmosphere, TiEMPO utilizes the Atmospheric Transmission at Microwave (ATM) model[14] to simulate the spectral dependence and the Astronomical Radio Interferometer Simulator (ARIS) model[15–17] to simulate the spatial/temporal variations. Compared with the Time Ordered Astrophysics Scalable Tools (TOAST)[18] package developed independently by the cosmic microwave background community, TiEMPO is primarily motivated by ultra-wideband spectroscopy of astronomical objects and includes a physical noise model of microwave kinetic inductance detectors (MKIDs). TiEMPO is distributed as an open-source Python package, and the scripts are available on a public repository[19] to encourage further use and development by the astronomical community to study cases for different telescope/instrument systems.

2 TiEMPO Model

2.1 *Overview*

TiEMPO is an end-to-end model, containing models of the astronomical source, the atmosphere, the telescope, the cryogenic instrument optics, and an integrated superconducting spectrometer with MKIDs (see Fig. 2). The details of the TiEMPO model can be found in Refs. 21 and 22, and the source code is publicly available.[19] In the following we provide an overview of the modules, in the order of signal propagation from the astronomical source to the detector.

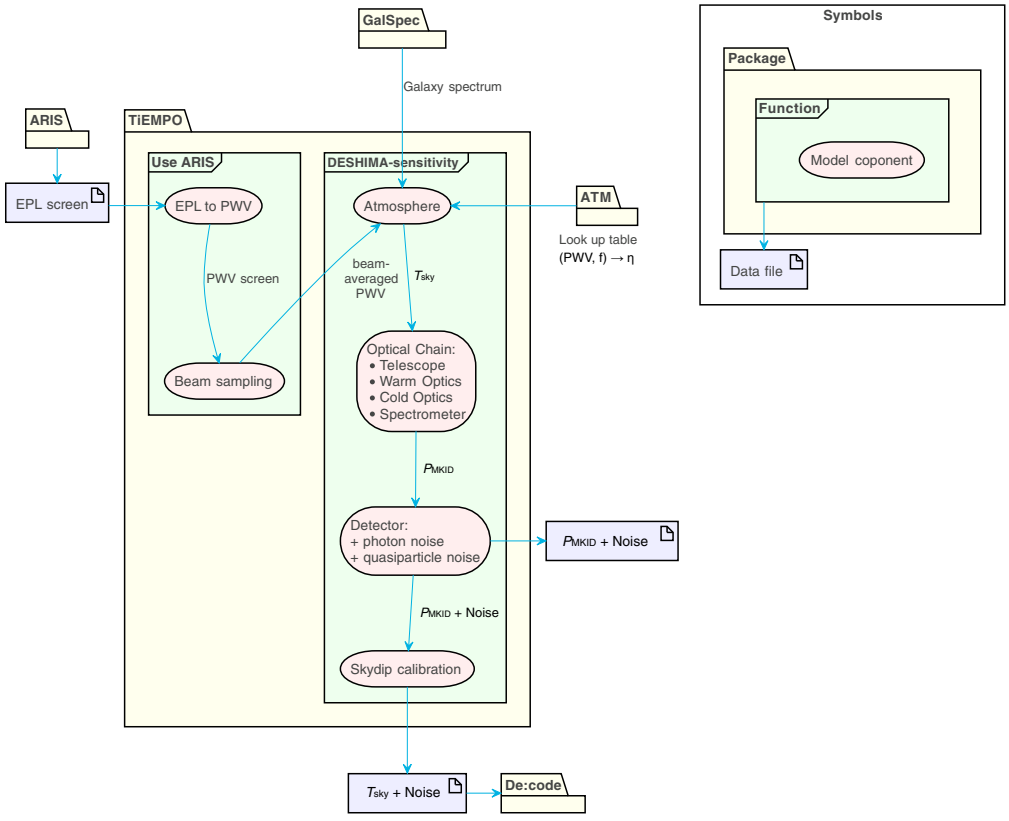

Fig. 2 System diagram of TiEMPO, showing each component with its input and output. TiEMPO depends on external packages ARIS,[15,16] ATM,[14] and GalSpec.[20] TiEMPO outputs calibrated sky brightness temperature T_{sky} and detector output P_{MKID}, which contains photon noise, quasiparticle recombination noise, and atmospheric noise. The output timestream data can be analyzed by post-processing software such as De:code.[13]

2.2 *Spectrum of a Dusty High-Redshift Galaxy*

The galaxy spectrum was created using the GalSpec package,[20] which we distribute as an open-source Python package that can be used outside of TiEMPO. Our goal is to create a galaxy template that is similar to the types of galaxies that we will be trying to detect with DESHIMA and with which we are able to model the potential future science cases. As such, we use an empirical approach to the creation of a galaxy spectrum, combining the continuum shape and spectral line luminosities from recent studies of observed local and high-redshift galaxies. The continuum is based on the two-component modified-black body fit to 24 galaxies at $z > 2$ with Herschel (250, 350, and 500 μm) and SCUBA-2 (850 μm) fluxes.[23,24] Here, we normalize the spectrum to the total far-infrared luminosity by integrating the spectrum from 8 to 1000 μm. The spectral lines are simulated with a more creative approach that can be tailored to specific science goals. Relatively shallow observations, aimed at detecting atomic lines and CO, are simulated using spectral line luminosity scaling relations. Here we use the scaling relations from Ref. 25 for atomic lines and Ref. 26 for both CO and [CI] lines. The scaling relations of Ref. 25 are based on local star-forming and ultra-luminous infrared galaxies and high-redshift submm galaxies, whereas the scaling relations of Ref. 26 are based mostly on local galaxies. Deeper observations might resolve more complex molecular lines in both emission and absorption, such as H_2O, HCN, HCO^+, CH^+, NH, NH_2, OH^+, and HF. These species are only incidentally seen at high redshift (e.g., Refs. 27 and 28), and thus we rely on the line detections in the nearby ULIRG Arp 220 to supplement our spectrum for these molecular species.[29] Here, instead of scaling to the far-infrared luminosity, we scale the line brightness to the observed continuum at the line's frequency. For this complete galaxy spectrum, we note that the brightness of these spectral lines is a probe of the conditions of the interstellar medium. As such, the line brightnesses (and even the continuum) are known to vary by up to 1 dex from source to source, which must be taken into account when applying for the necessary observation time or detection limits. Throughout this study, we assume a uniform line velocity width of 600 $\mathrm{km\,s^{-1}}$ (full width half maximum), which is found to be the mean for typical submillimeter galaxy[30] and in line with recent observations of South Pole Telescope and bright Herschel sources.[31–33]

2.3 *Creation of the Atmosphere Screen*

Our goal here is to obtain the line-of-sight transmittance of the atmosphere η_{atm}, which depends on the time t and telescope pointing angle (θ, ϕ). Here, θ and ϕ are the elevation and azimuth angles of the telescope pointing, respectively. We start from the observation that the mm–submm η_{atm} at zenith ($\theta = 90$ deg) is correlated with chiefly one variable, the precipitable water vapor (PWV).[34] Water vapor not only absorbs the submm waves but also introduces an extra path length (EPL) that is dependent on the line-of-sight PWV.[35] ARIS[15,16] uses a set of spatial structure functions[36] to produce a phase screen, i.e., a two-dimensional map of EPL as shown in the left panel of Fig. 3. Input parameters of ARIS include the inner and outer scales and exponents, the spatial size and resolution of the screen, and the root-mean-square (RMS) fluctuation of EPL in combination with a distance. Further details about the parameters can be found in Ref. 16, and typical values for the Atacama Large Millimeter–Submillimeter Array (ALMA) site are reported in Ref. 17.

TiEMPO converts an EPL screen to a PWV screen, using the following relation derived from the Smith–Weintraub constants[37] of EPL and the ideal gas law (see Ref. 21 for details), which is given as

$$d\mathrm{EPL} = 10^{-6}\rho R\left(k_2 + \frac{k_3}{T}\right) d\mathrm{PWV} \sim 6.587 \cdot d\mathrm{PWV}. \tag{1}$$

Here, $k_2 = 70.4 \pm 2.2$ $\mathrm{K\,mbar^{-1}}$ and $k_3 = (3.739 \pm 0.012) \cdot 10^5$ $\mathrm{K^2\,mbar^{-1}}$ are the Smith–Weintraub constants,[37] $\rho = 55.4 \cdot 10^3$ $\mathrm{mol\,m^{-3}}$ is the number density of molecules in liquid water, $R = 8.314 \cdot 10^{-2}$ $\mathrm{mbar\,m^3\,K^{-1}\,mol^{-1}}$ is the gas constant, and approximately $T = 275$ K is the physical temperature of the atmosphere. Note that dEPL and dPWV are differences from arbitrary mean values of the optical path length and PWV, respectively. In TiEMPO the user can

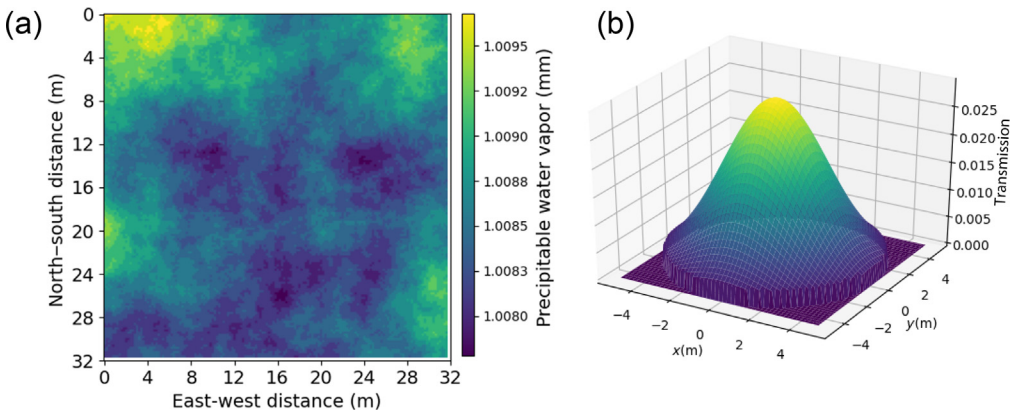

Fig. 3 (a) Colormap of the output of ARIS for a 32 m × 32 m sky window converted to PWV with Eq. (1). (b) The truncated Gaussian that is used as the telescope beam shape in the model. The volume of the Gaussian is normalized to unity, and it is truncated at a radius of 5 m, where its height is 10% of its peak height (Video 1, Mp4, 1070 KB [URL: https://doi.org/10.1117/1.JATIS.8.2.028005.1]).

specify a mean PWV, around which the PWV fluctuates according to the ARIS-modeled EPL and Eq. (1). The mean PWV can be set to a constant or a vector that represents a slowly changing weather condition. The created PWV screen moves spatially in one direction, at the user-specified wind velocity, assuming that the structure of phase fluctuations is invariant when the atmosphere moves with the wind.[38] See Fig. 3(a) and Video 1 for an example of the moving atmosphere created in TiEMPO.

2.4 *Sampling of the Atmosphere by the Telescope Near-Field Beam*

The water vapor in the atmosphere above the Atacama Desert is contained mostly in the layer up to ∼1 km from ground,[39] which is well within the near field of the telescope. Therefore, the beam pattern at this height has a similar pattern to the power distribution over the primary mirror of the telescope. In this study, we assumed that the PWV screen is 1 km above the telescope. For simulating DESHIMA on Atacama Submillimeter Telescope Experiment (ASTE) using TiEMPO, we assumed a Gaussian power pattern as shown in Fig. 3(b), which drops to −10 dB at the telescope radius of 5 m. The PWV map created in Sec. 2.3 is filtered with this beam pattern, so the received power from the atmosphere is a weighted average within the beam. The user may include an arbitrary beam pattern in TiEMPO when detailed information is available from the design or measurement.

2.5 *Far-Field Beam of the Telescope*

The far-field telescope beam is modeled by two properties: the main beam solid angle Ω_{MB} and the main beam efficiency η_{MB}.[1,40] Ω_{MB} represents the solid angle of the beam excluding the side lobes. η_{MB} is the fraction of the beam contained in the main beam, out of the total reception pattern. The (total) beam solid angle, with the side lobes included, is then given by

$$\Omega_{\mathrm{A}} = \frac{\Omega_{\mathrm{MB}}}{\eta_{\mathrm{MB}}}. \tag{2}$$

We use the beam solid angle to define the effective aperture area as

$$A_{\mathrm{e}} = \frac{\lambda^2}{\Omega_{\mathrm{A}}}, \tag{3}$$

where λ is the wavelength. Now, we express the aperture efficiency η_{A} as

$$\eta_A = \frac{A_e}{A_p} = \frac{\eta_{MB}}{\Omega_{MB}} \frac{\lambda^2}{A_p}, \tag{4}$$

where A_p is the physical area of the telescope primary mirror. From these quantities, the single-mode power density (in $W\,Hz^{-1}$) of the astronomical source is calculated as

$$P_f = \frac{1}{2} F_f A_e, \tag{5}$$

where F_f denotes the flux density in $W\,m^{-2}\,Hz^{-1}$ ($= 10^{26}$ Jy) and the factor $1/2$ compensates for the fact that the flux density is calculated using two polarizations, but the power density that TiEMPO calculates is for single-polarization assuming the coupling of the signal to a single-mode (on-chip) antenna and transmission line.[2]

2.6 *Radiative Transfer*

For calculating the single-mode radiation transfer from the astronomical source to the detector, a subset of the DESHIMA-sensitivity software[41] was used. Each component in the optical chain is modeled with a black body power density and a transmission factor η_i. The single-mode power density of a black body is equivalent to the Johnson–Nyquist noise and is given by

$$P_f = \frac{hf}{e^{\frac{hf}{k_B T}} - 1}. \tag{6}$$

Here, h is the Planck constant, f is the frequency, k_B is the Boltzmann constant, and T is the physical temperature of the emitter.[42] The spectral power before the detector is computed by cascading the radiation transfer of each component as

$$P_{f,\mathrm{out}} = \eta_i P_{f,\mathrm{in}} + (1 - \eta_i) P_{f,i}, \tag{7}$$

where $P_{f,\mathrm{out}}$ is the power density of the radiation that comes out of the component, $P_{f,\mathrm{in}}$ is the power density of the radiation going in, η_i is the transmittance of the component, and $P_{f,i}$ is the power density of the component.

2.7 *Spectrometer*

TiEMPO is able to model any direct-detection (imaging-)spectrometer that couples the wideband input power into one or more spectral channels. Examples include integrated filterbank spectrometers that use a filterbank[1–3] or an integrated grating[4,5] and optical grating spectrometers. Currently, TiEMPO takes five spatial pixels (a center pixel pointed toward the astronomical source, and top, bottom, right, and left pixels viewing only the atmosphere) to simulate position-switching observations, but the pixel count can be increased to model multi-pixel imaging arrays. If the number of spectral channels per pixel is set to unity, then the model can represent a monochromatic imaging camera.

TiEMPO can import the spectral response of each detector, obtained from the design[43] or a measurement.[44] Here, we assumed a simple Lorentzian-shaped spectral transmission, which is a good approximation for a filterbank channel,[2] or a detector behind an optical (or substrate-integrated) grating.[5] The frequency dependence was implemented by dividing the frequency range of 210 to 450 GHz (10 GHz wider on each side than the nominal DESHIMA 2.0 band, to take into account power coupling from outside of the band) into 1500 bins. The resulting efficiency is used to compute the power density with the radiation transfer equation, Eq. (7). Finally, the power in each bin is calculated as

$$P_{\mathrm{bin}\,i} = \Delta f P_{f,\mathrm{bin}\,i}. \tag{8}$$

Note that the $P_{\text{bin}\,i}$ in Eq. (8) is the expected (i.e., noiseless) value of the power. To calculate the frequency-integrated power detected by each detector at each moment t, $P_{\text{MKID}}(t)$, we must consider noise (see Sec. 2.8).

2.8 *Detected Power and Noise*

The best possible sensitivity of a pair-breaking detector like an MKID is set by the photon noise and quasiparticle recombination noise. The commonly-used narrow-band approximation for the noise equivalent power (NEP) limited by photon- and recombination-noise is given by[1]

$$\text{NEP}_{\text{MKID}} = \sqrt{2\overline{P_{\text{MKID}}}(hf + \overline{P_{\text{MKID}}}/\Delta f) + 4\Delta_{\text{Al}}\overline{P_{\text{MKID}}}/\eta_{\text{pb}}}. \tag{9}$$

Here, $\overline{P_{\text{MKID}}}$ is the expected value of the power absorbed by the MKID, $\Delta_{\text{Al}} = 188\ \mu\text{eV}$ ($\sim 91\ \text{GHz} \cdot h/2$) is the superconducting gap energy of aluminum, and approximately $\eta_{\text{pb}} = 0.4$ is the pair-breaking efficiency.[45] In TiEMPO we use the more general, integral form of the NEP[46] to take into account a frequency-dependent optical efficiency over a wide bandwidth, for each detector of the spectrometer. This method also accounts for photon-bunching of the wideband signal. Because the fluctuations in energy in different spectral bins are uncorrelated,[47] we can calculate the standard deviation in power for each spectral bin per sampling rate ($1/f_{\text{sampling}}$) from

$$\sigma = \text{NEP}_{\text{MKID}}\sqrt{\frac{1}{2}f_{\text{sampling}}}, \tag{10}$$

and add those together to obtain the combined detector output, as given by

$$P_{\text{MKID}} = \sum_{i=1}^{\#\text{bins}} P_{\text{bin}\,i,\,\text{with noise}}. \tag{11}$$

Note that this is equivalent to calculating the detector NEP directly from the integral, which is expressed as

$$\text{NEP}^2_{\text{MKID}} = \int 2P_f(hf + P_f) + 4\Delta_{\text{Al}}P_f/\eta_{\text{pb}}\mathrm{d}f. \tag{12}$$

The integration over a wide bandwidth taking the filter spectral transmission into account is especially relevant for spectral channels that are near strong emission lines and absorption bands of the atmosphere.[10]

2.9 *Sky Temperature Calibration*

After computing the noise-added power that is measured by the MKIDs, we want to relate this back to the original signal from the sky. We do this by expressing the received power in sky brightness temperature T_{sky}: the physical temperature of a black body that would have the same intensity as the semitransparent sky.[1] To this end we take the Johnson–Nyquist equation, which is given by

$$T_{\text{sky}} = \frac{hf}{k_{\text{B}}\ \ln\left(\frac{hf}{P_f} + 1\right)}. \tag{13}$$

To relate the MKID power P_{MKID} to T_{sky}, TiEMPO internally performs a skydip simulation[10] using the DESHIMA-sensitivity[41] script. A skydip is a series of measurements in which the telescope "dips" from a high elevation (pointing at zenith) to a low elevation (pointing almost horizontally). When the elevation is lower, the telescope looks through a thicker layer of atmosphere, increasing the opacity and hence the power and the sky temperature, allowing us to

construct a relationship between the two. In our simulations, we use elevation values in the range of $\theta = 20$ deg to 90 deg. The power and sky temperature data are interpolated for each channel and saved in the model. TiEMPO reuses these interpolation curves, so they only need to be created once. For further details on the numerical skydip calibration, see Ref. 21.

3 Comparing a TiEMPO Simulation with On-Sky DESHIMA 1.0 Measurements

To verify the TiEMPO model, we made a simulation of an atmosphere observation using input parameters that resemble a real measurement done with the DESHIMA spectrometer on the ASTE telescope.[48] DESHIMA is an integrated superconducting spectrometer with MKID detectors. The first generation of DESHIMA, which we will hereafter call DESHIMA 1.0,[1] has an instantaneous band of 332 to 377 GHz, with a frequency spacing of $f/\Delta f = 380$ approximately. (The half-power bandwidth of each filter is $f/\Delta f = 300$ on average.[2]) ASTE is a 10-m Cassegrain reflector located on the Pampa la Bola plateau of the Atacama Desert in northern Chile, at an altitude of 4860 m. DESHIMA 1.0 was operated on ASTE during October to November 2017.[1] The measured response of the MKIDs was converted to sky brightness temperature T_{sky} using the skydip calibration method explained in detail in Ref. 10.

We use the data taken from a measurement on November 17, 2017, in which the telescope was pointed close to zenith ($\theta = 88$ deg) for 3000 s. The PWV measured with the radiometer of the ALMA was 1.7 mm at the beginning of the measurement, corresponding to a ~350 GHz sky brightness temperature of ~80 K. In Fig. 4, we show the time-evolution of the measured T_{sky} taken with the 355 GHz channel of DESHIMA 1.0 (blue curve). The DESHIMA measurement indicates that the PWV dropped continuously over the course of the measurement, from ~1.7 to ~1.3 mm.

We ran a few simulations in TiEMPO to fine-tune the input parameters to achieve good agreement between simulation and measurement in the noise-equivalent-flux-density (NEFD) spectrum, which we present in Fig. 5. The resulting TiEMPO-simulated time trace of measured T_{sky} for the 355 GHz channel is compared with that of the DESHIMA 1.0 measurement in Fig. 4. Qualitatively, both curves show two types of fluctuations that are behaving similarly: the low-frequency and large-amplitude fluctuations are due to atmospheric noise, whereas the high-frequency and small-amplitude fluctuations are due to photon noise and quasiparticle recombination noise.

To compare the noise in the simulation and measurement more quantitatively, we take the noise spectrum of the time traces. Before taking the spectrum, we convert T_{sky} to flux density as

$$F_f(T_{\mathrm{sky}}) = \frac{2\Omega_{\mathrm{MB}}}{\eta_{\mathrm{MB}}\lambda^2\eta_{\mathrm{atm}}} \frac{hf}{e^{\frac{hf}{kT_{\mathrm{sky}}}} - 1}. \tag{14}$$

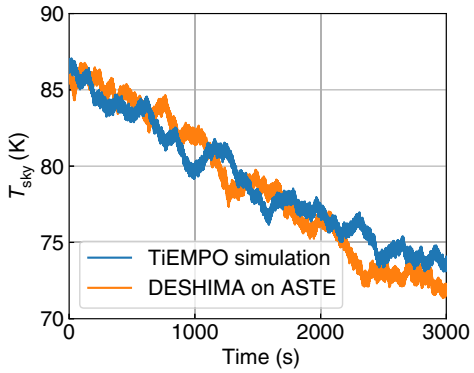

Fig. 4 Time stream of the measured T_{sky} at 355 GHz, for a TiEMPO simulation (blue) and DESHIMA/ASTE observation on the ASTE telescope (orange).

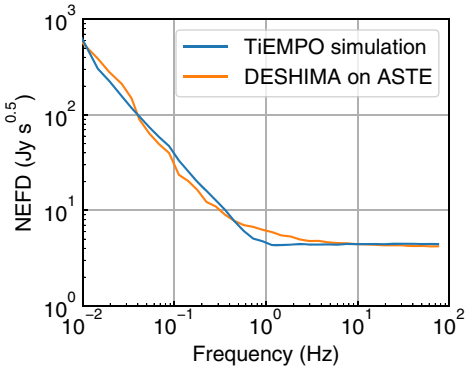

Fig. 5 NEFD spectra, derived from the power spectral densities of the time-series data presented in Fig. 4, for the TiEMPO simulation (blue) and DESHIMA/ASTE observation (orange).

Subsequently, we calculate the noise equivalent flux density (NEFD) by

$$\mathrm{NEFD} = \sqrt{\frac{\mathrm{PSD}\{F_f(t)\}}{2}}, \tag{15}$$

where PSD{} denotes the operation of taking the power spectral density. The factor $\sqrt{2}$ is introduced because we define the NEFD for an integration time of 1 s. In Fig. 5, we show the resulting NEFD spectra for the simulation and measurement. At $\lesssim$1 Hz, the NEFD curves exhibit the $1/f$-noise generated by the atmospheric fluctuations. At $\gtrsim$1 Hz, the spectra flatten out to the white photon (and recombination) noise level. This form of noise spectra is often seen in mm–submm observations.[49] The simulation agrees well with the measurement for both the photon (and recombination) noise level and the atmospheric $1/f$-noise. Near the $1/f$ knee frequency at $\sim$1 Hz, the measurement shows a slight excess compared with the TiEMPO simulation. This is most likely the contribution from the dielectric two-level system noise of the MKIDs, which can also be included in TiEMPO in the future. Examples of early implementations can be found in Refs. 12 and 44.

We plot the photon and recombination noise NEFD of all 49 simulated channels in Fig. 6, together with the measured NEFD of DESHIMA 1.0 on ASTE based on actual measurements of astronomical lines.[1] Considering the above-mentioned simplified filter model, as well as the fact that the measurements were taken across nights with different atmospheric conditions,[1] the agreement is good. A more detailed analysis taking into account the measured characteristics of each channel[44] finds an even closer agreement.

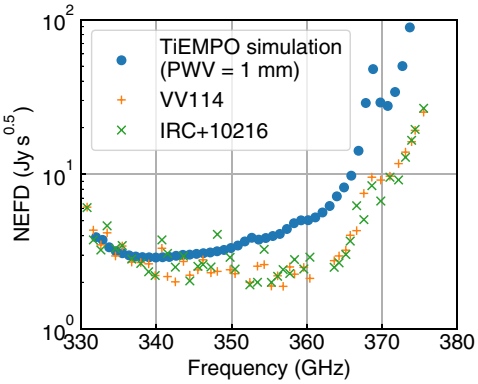

Fig. 6 NEFD at the flat photon-noise level for a TiEMPO-simulation with the PWV set to 1.0 mm, compared with the NEFD of DESHIMA 1.0 based on actual detection of astronomical emission lines, from the luminous infrared galaxy VV 114 and the post-asymptotic giant branch star IRC+10216.[1] The peaks at around 353 and 368 GHz are lines of O_3 and O_2, respectively.

In summary of this section, the output of TiEMPO resembles the on-sky measurement of DESHIMA 1.0, in both the time domain and the frequency domain. The end-to-end system sensitivity inferred from the simulation is in good agreement with the actual measurement of astronomical sources performed by DESHIMA 1.0 on ASTE.

4 TiEMPO Simulation of Observing a High-Redshift Galaxy with DESHIMA 2.0 on ASTE

As an example application of TiEMPO, we simulate the observation of a virtual luminous dusty galaxy ($L_{\mathrm{FIR}} = 10^{13.7} L_{\odot}$) at redshift $z = 4.43$ and velocity width 600 km s^{-1} using the DESHIMA 2.0 spectrometer on the ASTE telescope. DESHIMA 2.0 is an upgrade of DESHIMA 1.0, which is currently under development.[50] The target instantaneous frequency coverage is 220 to 440 GHz, with a frequency spacing and half-power channel bandwidth of $f/\Delta f = 500$. The system will include a rotating mirror in the cabin optics that enables position switching on the sky at a rate of up to 10 Hz. Assuming the use of this beam chopper, we simulated a so-called ABBA chop-nod observing technique[22,51] with a beam-chopping frequency of 10 Hz between on-source and off-source positions and a nodding cycle of 60 s to subtract the atmospheric emission from the spectrum. The total simulated observation time was 1 h. The input spectrum of the galaxy was simulated using GalSpec. The telescope elevation angle was kept constant at 60 deg, and the weather condition was set to mean PWV = 1.0 mm; RMS fluctuation of the EPL for 1 km distance of $\sigma_{\mathrm{EPL}} = 50$ μm, which is typical for the ALMA site [see for example Fig. 2(b) in Ref. 17]; and wind velocity = 9.6 m s^{-1}.

The resulting spectrum after applying the ABBA atmosphere removal scheme is presented in Fig. 7. The top panel shows the spectrum in ΔT_{sky}, that is, before correcting for atmospheric absorption. The spectrum shows the detection of the redshifted [CII] line at 350 GHz and the dust

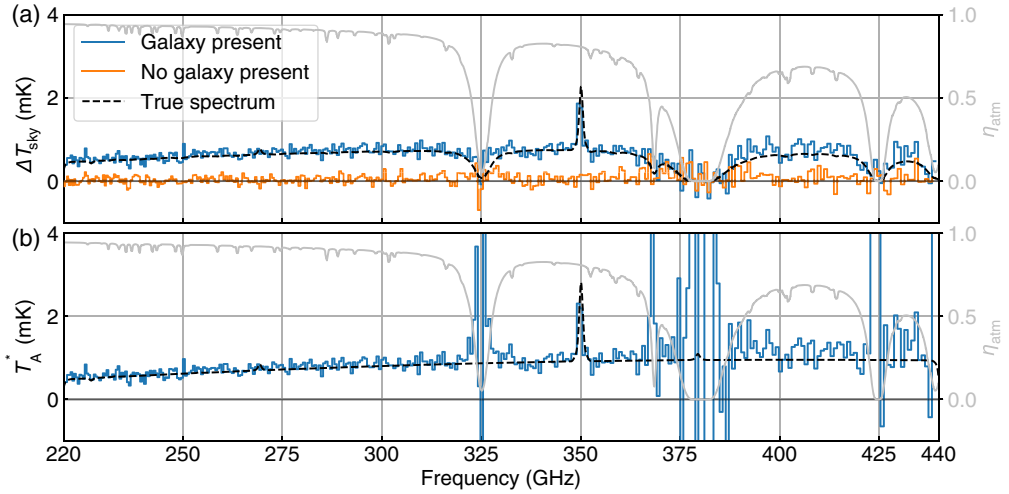

Fig. 7 TiEMPO-simulated detection of a high-redshift dusty galaxy with the upcoming DESHIMA 2.0 instrument on ASTE. The galaxy spectrum was simulated using GalSpec, with input parameters as follows: far-infrared bolometric luminosity $10^{13.7} L_{\odot}$; redshift $z = 4.43$; and velocity width 600 km s^{-1}. The total observing time was 60 min, out of which half was pointing on-source. (a) ΔT_{sky}, which is the difference in sky temperature T_{sky} between on-source and off-source obtained with the ABBA chop-nod method. The blue spectrum is the result of placing a galaxy at the on-position, and the orange spectrum is the result of no galaxy being present. The dashed curve is the expected spectrum of the galaxy, multiplied by the atmospheric transmittance η_{atm} (gray) and smoothed with a Lorentzian window of $f/\Delta f = 500$ to account for the resolving power of the spectrometer. (b) The atmosphere-corrected antenna temperature $T_{\mathrm{A}}^{*} = \Delta T_{\mathrm{sky}}/\eta_{\mathrm{atm}}$. The blue curve shows the simulated spectrum, and the dashed curve is what is expected directly from the input galaxy spectrum.

continuum emission. In the same figure, we show that a reference simulation without a galaxy yields a zero-centered spectrum as expected. Dividing the ΔT_{sky}-spectrum by the frequency-dependent atmospheric transmittance η_{atm} yields the spectrum presented in the bottom panel, where the scale is now atmosphere-corrected antenna temperature T_{A}^{*}. In this way, TiEMPO is able to simulate end-to-end observations of future instruments and forecast their scientific products. The TiEMPO data can also be used to optimize observing strategies and signal-processing techniques before the instrument is deployed.

5 Conclusion and Future Prospects

We have presented the TiEMPO model and verified its applicability by comparing its output with on-sky measured data and simulating the operation of a future instrument. The TiEMPO model is highly parametrized and modular, so it can be adjusted to different observation techniques, telescopes, and instruments. This can be done by either simply adjusting the input parameters or by relatively simple modifications of the Python code. For example, some of the authors have adapted TiEMPO to simulate scan-mapping observations[52] or include excess detector noise.[44] TiEMPO can also import arbitrary frequency-dependent transmission curves from models or measurements to replace the Lorentzian filter transmission used in this article.[44] The time-dependent telescope elevation can be given as a user-specified vector. If the detector is not a pair-breaking type (e.g., superconducting transition-edge sensors), then the recombination noise term can be omitted in Eq. (9).

It would seem especially interesting to use TiEMPO for the design and optimization of large mm–submm telescopes, such as the Large Submillimeter Telescope[7] and Atacama Large Aperture Submillimeter Telescope,[6] as well as for optimizing instruments and observing techniques on existing large telescopes like the Large Millimeter Telescope.[53] These telescopes have diameters in the range of 30 to 50 m, so they sample a larger column of atmosphere that contains a larger number of patches of water vapor that can influence the noise behavior. The combination of TiEMPO and ARIS can already simulate observations with telescopes of these sizes, in combination with the wideband direct detection imaging spectrometers that are considered to be candidates for future instruments. Note that the current TiEMPO models only the transmittance of the atmosphere, and it does not model the wavefront distortion caused by the dynamical and spatially dependent EPL.[54] Because ARIS provides an EPL screen, this would be an interesting direction for future development.

Acknowledgments

This paper is based on the scientific content previously reported in SPIE proceedings.[55] We would like to thank Yoshiharu Asaki for providing us with knowledge about the Atacama atmosphere and the ARIS model, including multiple upgrades of ARIS to enable the use of large phase screens for TiEMPO. We would also like to thank Henry Kool for the optimization of the computation server used for this study. Most of the development and validation of TiEMPO was carried out as the TU Delft Bachelor End Projects of E.H. and Y.R. S.A.B. completed the development and published the TiEMPO package as part of her TU Delft Master End Project. A.E. was supported by the Netherlands Organization for Scientific Research NWO (Vidi Grant No. 639.042.423). J.J.A.B. was the supported by the European Research Counsil ERC (ERC-CoG-2014 - Proposal No. 648135 MOSAIC). Y.T. and T.J.L.C.B. were supported by the Japan Society for the Promotion of Science JSPS (KAKENHI Grant No. JP17H06130). The ASTE telescope is operated by the National Astronomical Observatory of Japan (NAOJ).

Code Availability

TiEMPO,[19] GalSpec,[20] DESHIMA-sensitivity,[41] and De:code[13] are all available as Python packages and distributed on a public repository.

References

1. A. Endo et al., "First light demonstration of the integrated superconducting spectrometer," *Nat. Astron.* **3**, 989–996 (2019).
2. A. Endo et al., "Wideband on-chip terahertz spectrometer based on a superconducting filterbank," *J. Astron. Telesc. Instrum. Syst.* **5**, 035004 (2019).
3. K. S. Karkare et al., "Full-array noise performance of deployment-grade superspec mm-wave on-chip spectrometers," *J. Low Temp. Phys* **199**(3–4), 849–857 (2020).
4. P. A. R. Ade et al, "The experiment for cryogenic large-aperture intensity mapping (EXCLAIM)," *J. Low Temp. Phys* **199**(3–4), 1027–1037 (2020).
5. E. M. Barrentine et al., "Design and performance of a high resolution μ-spec: an integrated sub-millimeter spectrometer," *Proc. SPIE* **9914**, 99143O (2016).
6. P. D. Klaassen et al., "The Atacama Large Aperture Submillimeter Telescope (AtLAST)," *Proc. SPIE* **11445**, 114452F (2020).
7. R. Kawabe et al., "New 50-m-class single-dish telescope: Large Submillimeter Telescope (LST)," *Proc. SPIE* **9906**, 990626 (2016).
8. H. Terry et al., "The CCAT-prime submillimeter observatory," *Bull. Am. Astron. Soc.* **51**, 213 (2019).
9. A. Taniguchi et al., "A new off-point-less observing method for millimeter and submillimeter spectroscopy with a frequency-modulating local oscillator," *Publ. Astron. Soc. Jpn.* **72**, 2 (2020).
10. T. Takekoshi et al., "DESHIMA on ASTE: on-sky responsivity calibration of the integrated superconducting spectrometer," *J. Low Temp. Phys* **199**, 231–239 (2020).
11. A. Taniguchi et al., "A data-scientific noise-removal method for efficient submillimeter spectroscopy with single-dish telescopes," *Astron. J.* **162**, 111 (2021).
12. S. Brackenhoff, "SPLITTER: a data model and algorithm for detecting spectral lines and continuum emission of high-redshift galaxies using DESHIMA 2.0," MSc Thesis, Delft University of Technology (2021).
13. A. Taniguchi and T. Ishida, "De:code," https://doi.org/10.5281/zenodo.5733835.
14. J. R. Pardo, J. Cernicharo, and E. Serabyn, "Atmospheric transmission at microwaves (ATM): an improved model for millimeter/submillimeter applications," *IEEE Trans. Antennas Propag.* **49**(12), 1683–1694 (2001).
15. Y. Asaki et al., "Verification of the effectiveness of VSOP-2 phase referencing with a newly developed simulation tool, aris," *Publ. Astron. Soc. Jpn.* **59**(2), 397–418 (2007).
16. Y. Asaki et al., "Simulation series of a phase calibration schemewith water vapor radiometers for the Atacama compact array," Technical Report, ALMA MEMO No. 535 – http://library.nrao.edu/alma.shtml (2005).
17. S. Matsushita et al., "Alma long baseline campaigns: phase characteristics of atmosphere at long baselines in the millimeter and submillimeter wavelengths," *Publ. Astron. Soc. Pac.* **129**(973), 035004 (2017).
18. T. Kisner et al., "hpc4cmb/toast: update pybind11."
19. E. Huijten and S. A. Brackenhoff, "tiempo_deshima," https://doi.org/10.5281/zenodo.4639721.
20. T. J. L. C. Bakx and S. A. Brackenhoff, "GalSpec," https://doi.org/10.5281/zenodo.4279062.
21. E. Huijten, "TiEMPO: time-dependent end-to-end model for post-process optimization of the DESHIMA spectrometer," Delft University of Technology Bachelor's Thesis (2020).
22. Y. Roelvink, "Simulation of a high-redshiftline-emitting galaxy detection with DESHIMA using TiEMPO," Delft University of Technology Bachelor's Thesis (2020).
23. T. J. L. C. Bakx et al., "The Herschel Bright Sources (HerBS): sample definition and SCUBA-2 observations," *Mon. Not. R. Astron. Soc.* **473**, 1751–1773 (2018).
24. T. J. L. C. Bakx et al., "Erratum: the Herschel Bright Sources (HerBS): sample definition and SCUBA-2 observations," *Mon. Not. R. Astron. Soc.* **494**, 10–16 (2020).
25. M. Bonato et al., "Exploring the early dust-obscured phase of galaxy formation with blind mid-/far-infrared spectroscopic surveys," *Mon. Not. R. Astron. Soc.* **438**, 2547–2564 (2014).

26. J. Kamenetzky et al., "L'co/LFIR relations with CO rotational ladders of galaxies across the Herschel SPIRE archive," *Astrophys. J.* **829**, 93 (2016).
27. J. S. Spilker et al., "Fast molecular outflow from a dusty star-forming galaxy in the early Universe," *Science* **361**, 1016–1019 (2018).
28. S. Berta et al., "Close-up view of a luminous star-forming galaxy at z = 2.95," *Astron. Astrophys.* **646**, A122 (2021).
29. N. Rangwala et al., "Observations of Arp 220 using Herschel-SPIRE: an unprecedented view of the molecular gas in an extreme star formation environment," *Astrophys. J.* **743**, 94 (2011).
30. M. S. Bothwell et al., "A survey of molecular gas in luminous sub-millimetre galaxies," *Mon. Not. R. Astron. Soc.* **429**, 3047–3067 (2013).
31. C. Reuter et al., "The complete redshift distribution of dusty star-forming galaxies from the SPT-SZ survey," *Astrophys. J.* **902**, 78 (2020).
32. T. J. L. C. Bakx et al., "IRAM 30-m-EMIR redshift search of z = 3-4 lensed dusty starbursts selected from the HerBS sample," *Mon. Not. R. Astron. Soc.* **496**, 2372–2390 (2020).
33. R. Neri et al., "NOEMA redshift measurements of bright Herschel galaxies," *Astron. Astrophys.* **635**, A7 (2020).
34. Y. Sewnarain Sukul, "Principal component analysis on atmospheric noise measured with an integrated superconducting spectrometer," Delft University of Technology Bachelor's Thesis (2019).
35. A. R. Thompson, J. M. Moran, and G. W. Swenson, *Interferometry and Synthesis in Radio Astronomy*, 3rd ed., Springer, Cham (2017).
36. A. Dravskikh and A. Finkelstein, "Tropospheric limitations in phase and frequency coordinate measurements in astronomy," *Astrophys. Space Sci.* **60**(2), 251–265 (1979).
37. E. K. Smith and S. Weintraub, "The constants in the equation for atmospheric refractive index at radio frequencies," *Proc. IRE* **41**(8), 1035–1037 (1953).
38. A. Gurvich et al., *Atmospheric Turbulence and Radio Wave Propagation*, Nauka, Moscow (1967).
39. R. Giovanelli et al., "The optical/infrared astronomical quality of high Atacama sites. II. Infrared characteristics," *Publ. Astron. Soc. Pac.* **113**(785), 803 (2001).
40. T. Wilson, K. Rohlfs, and S. Huettemeister, *Tools of Radio Astronomy, Astronomy and Astrophysics Library*, 5th ed., Springer-Verlag, Berlin Heidelberg (2009).
41. A. Taniguchi et al., "DESHIMA-sensitivity," https://doi.org/10.5281/zenodo.5968304.
42. H. Nyquist, "Thermal agitation of electric charge in conductors," *Phys. Rev.* **32**(1), 110 (1928).
43. A. Pascual Laguna et al., "Terahertz band-pass filters for wideband superconducting on-chip filter-bank spectrometers," *IEEE Trans. Terahertz Sci. Technol.* **11**, 635–646 (2021).
44. K. Marthi, "Modelling kinetic inductance detectors and associated noise sources," 2020, University of Groningen Internship Report, http://fse.studenttheses.ub.rug.nl/id/eprint/23044.
45. T. Guruswamy, D. J. Goldie, and S. Withington, "Quasiparticle generation efficiency in superconducting thin films," *Supercond. Sci. Technol.* **27**, 055012 (2014).
46. J. Zmuidzinas, "Thermal noise and correlations in photon detection," *Appl. Opt.* **42**(25), 4989 (2003).
47. P. L. Richards, "Bolometers for infrared and millimeter waves," *J. Appl. Phys.* **76**(1), 1–24 (1994).
48. H. Ezawa et al., "The Atacama Submillimeter Telescope Experiment (ASTE)," *Proc. SPIE* **5489**, 763–772 (2004).
49. A. Monfardini et al., "A dual-band millimeter-wave kinetic inductance camera for the IRAM 30 m telescope," *Astrophys. J. Suppl. Ser.* **194**, 24 (2011).
50. A. Pascual Laguna et al., "Wideband sub-mm wave superconducting integrated filter-bank spectrometer," in *44th Int. Conf. Infrared, Millimeter, and Terahertz Waves (IRMMW-THz)*, Paris, IEEE, pp. 1–2 (2019).
51. E. N. Archibald et al., "On the atmospheric limitations of ground-based submillimetre astronomy using array receivers," *Mon. Not. R. Astron. Soc.* **336**, 1–13 (2002).

52. S. Zaalberg, "Establishing a pointing calibration method for DESHIMA using TiEMPO," Delft University of Technology Bachelor's Thesis (2020).
53. D. H. Hughes et al., "The large millimeter telescope Alfonso Serrano: scientific operation of the LMT 50-m, first results and next steps," *Proc. SPIE* **10700**, 107000C (2018).
54. Y. Tamura et al., "Wavefront sensor for millimeter/submillimeter-wave adaptive optics based on aperture-plane interferometry," *Proc. SPIE* **11445**, 114451N (2020).
55. E. Huijten et al., "TiEMPO: open-source time-dependent end-to-end model for simulating ground-based submillimeter astronomical observations," *Proc. SPIE* **11453**, 114533C (2020).

Esmee Huijten is a master's student in physics at ETH Zurich. She received her bachelor's degree in applied physics and applied mathematics from TU Delft and developed TiEMPO during her bachelor's program. Her main interests are applying physics and mathematics to push the boundaries of technology and innovation, with a particular interest in mathematical modeling and solid state physics.

Yannick Roelvink received his bachelor's degree in applied physics from Delft University of Technology. Currently, he is a master's student in aerospace engineering with a major in embedded systems at the University of ISAE-SUPAERO in Toulouse, France. For his end-of-studies internship, he is working as a R&D engineer in "over the air key exchange for secure governmental satellite communication" within the innovation department of CYSEC, a cyber-security company based in Lausanne, Switzerland.

Stefanie A. Brackenhoff received her MSc degree in electrical engineering (cum laude) from TU Delft in 2021, specializing in signal processing. In her thesis, she developed a data model and algorithm for detecting spectral lines and continuum emission using DESHIMA 2.0. Before this, she received her BSc degrees in electrical engineering from TU Delft in 2019 and in astronomy from Leiden University in 2018. She is currently a PhD candidate at the University of Groningen, working on radio interferometry for constraining the epoch of reionization.

Akio Taniguchi is a postdoctoral researcher in the Division of Particle and Astrophysical Science at Nagoya University. He received his PhD from the University of Tokyo in 2018. He is contributing to the development of data analysis software for DESHIMA such as De:code and data analysis methods implemented on top of it. His research interests focus on the development of efficient spectroscopy for next-generation submillimeter single-dish telescopes based on data scientific approaches.

Tom J. L. C. Bakx is an ALMA post-doctoral researcher at Nagoya University. He received his undergraduate degree from TU Delft in 2014 and graduate degree from Cardiff University in 2018. His research focusses on submm observations of distant dust-obscured galaxies to trace their evolutionary pathways. To this end, he uses new instrumentation on single-dish telescopes, as well as the world's largest interferometers.

Kaushal B. Marthi received his MSc degree in astronomy with a specialization in instrumentation and informatics. He graduated from Rijksuniversiteit Groningen with a thesis researching the residual stresses present in metals used for optical instrumentation and completed internships at ASTRON and SRON. Prior to this, he received his BEng degree in mechanical engineering from the University of Sheffield. Currently, he is working as a junior software engineer at TJIP in Delft.

Stan Zaalberg was an applied physics BSc student in the Faculty of Applied Sciences at Delft University of Technolocy in 2020. In his BSc project, he applied TiEMPO to on-the-fly mapping observations, with the intended application of observing galaxy clusters through the Sunyaev–Zeldovich effect.

Anne-Kee Doing is a student at the Delft University of Technology. Currently, she is studying for a master's degree in engineering and policy analysis at the Faculty of Technology, Policy and Management. With this master's she learns how to provide policy advice based on self-made

models and data processing. All projects within this master's aim to contribute to the 17 sustainable development goals of the United Nations, an important aspect of the master's for her.

Jochem J. A. Baselmans is a senior instrument scientist at the SRON Netherlands Institute for Space Research and full professor in the THz sensing group at TU Delft. He leads the Dutch effort on the development of MKIDs; his main interests are ultra-sensitive devices for THz radiation detection and advanced on-chip imaging spectrometers for sub-THz imaging spectroscopy.

Kah Wuy Chin received his BS and MS degrees in astronomy from the University of Tokyo in 2017 and 2019, respectively. He contributed to data analysis and observation simulation in the DESHIMA projects. He is working on developing multi-color direct photon detectors using superconducting on-chip filter technology for a submillimeter astronomical camera as his PhD project.

Robert Huiting is a mechanical design engineer. He received his BS degrees in precision engineering in 2001 and technology management in 2003 from Hogeschool van Utrecht. He has been working as a design engineer for SRON Netherlands institute for space research since 2007. Prior to this, he has worked as a research engineer at the FOM institute for plasma physics for the XUV optics group. His experience from the last 6 years lies in designing instrumentation for ground based space research.

Kenichi Karatsu is an instrument scientist with SRON. He received his PhD in science from Kyoto University in 2011 with the study of proton spin structure at the RHIC-PHENIX experiment. In 2015, he joined the DESHIMA project at TU Delft/SRON. His main role is to lead the laboratory evaluation and telescope campaign of the instrument. His research interest is to develop an experimental instrument for revealing mysteries of the Universe.

Alejandro Pascual Laguna received his BSc degree in telecommunications engineering from the Universidad Pontificia Comillas, ICAI School of Engineering, Spain, in 2014. He received his MSc (cum laude) degree and PhD in electrical engineering from Delft University of Technology, the Netherlands, in 2016 and 2022, respectively. He currently works at SRON as a scientist specializing in on-chip solutions for efficient broadband submm wave spectrometric and imaging systems based on kinetic inductance detectors.

Yoichi Tamura is an associate professor of astronomy working in the Department of Physics, Nagoya University. His interests include galaxy formation, interstellar physics, and instrumentation for submillimeter astronomy. He received his PhD from the University of Tokyo in 2009. He joined the DESHIMA project when he was an assistant professor at the University of Tokyo (since 2011). In the present position (since 2017), he began a study on future large-aperture submillimeter telescopes.

Tatsuya Takekoshi is an assistant professor at Kitami Institute of Technology. He received his BS degree in physics and his MS degree and PhD in cosmoscience from Hokkaido University in 2008, 2010, and 2013, respectively. His research interests focus on investigating star formation process and activity in various galactic environments. He is also working on instrumental development using superconducting direct photon detectors for submillimeter astronomy.

Stephen J. C. Yates has been an instrument scientist since 2006 at SRON, the Netherlands Institute for Space Research. He received his PhD from the University of Bristol in 2003 and then worked at the CNRS-CRTBT (now Institut Neél) Grenoble on experimental low temperature techniques (2003 to 2006). His current interests include MKID development for sub-mm astronomy applications as well as a wider interest in device physics and superconductivity, optics, and full end to end instrument characterization and performance.

Maarten van Hoven is a lecturer of mathematics at TU Delft. He is a trained astrophysicist who received his PhD from Leiden University and performed post-doctoral research at Tel Aviv University before joining TU Delft. He has authored and co-authored several publications in

the fields of high energy astrophysics and observational astronomy. In his current capacity as lecturer, his main occupation is education development for undergraduate mathematics courses at TU Delft.

Akira Endo is an assistant professor at the THz Sensing Group of TU Delft. He is interested in 3D-observations of large cosmological volumes and the required development of (sub)millimeter-wave integral field units. He is the Dutch PI of the wideband DESHIMA spectrometer on the ASTE telescope. In 2022, he received the ERC Consolidator Grant to develop integral field units with many spaxels and to demonstrate it with astronomical observations (project TIFUUN).